

# The Suzaku Discovery of A Hard Power-Law Component in the Spectra of Short Bursts from SGR 0501+4516

Yujin E. NAKAGAWA,<sup>1</sup> Kazuo MAKISHIMA,<sup>2</sup> Teruaki ENOTO,<sup>3</sup>

<sup>1</sup>Research Institute for Science and Engineering, Waseda University, 17 Kikui-cho, Shinjuku-ku, Tokyo 162-0044  
yujin@aoni.waseda.jp

<sup>2</sup>Department of Physics, University of Tokyo, 7-3-1 Hongo, Bunkyo-ku, Tokyo 113-0033

<sup>3</sup>Kavli Institute for Particle Astrophysics and Cosmology, Department of Physics and SLAC National Accelerator Laboratory,  
Stanford University, Stanford, CA 94305, USA

(Received 2011 February 28; accepted 2011 June 24)

## Abstract

Using data with the Suzaku XIS and HXD, spectral studies of short bursts from the soft gamma repeater SGR 0501+4516 were performed. In total, 32 bursts were detected during the  $\sim 60$  ks of observation conducted in the 2008 August activity. Excluding the strongest one, the remaining 31 bursts showed an average 2–40 keV fluence of  $1.0_{-0.5}^{+0.3} \times 10^{-9}$  erg cm $^{-2}$ . A 1–40 keV spectrum summed over them leaves significant positive residuals in the HXD-PIN band with  $\chi^2/\text{d.o.f.} = 74/50$ , when fitted with a two-blackbody function. By adding a power law model, the fit became acceptable with  $\chi^2/\text{d.o.f.} = 56/48$ , yielding a photon index of  $\Gamma = 1.0_{-0.3}^{+0.4}$ . This photon index is comparable to  $\Gamma = 1.33_{-0.16}^{+0.23}$  (Enoto et al. 2010a) for the persistent emission of the same object obtained with Suzaku. The two-blackbody components showed very similar ratios, both in the temperature and the emission radii, to those comprising the persistent emission. However, the power-law to two-blackbody flux ratio was possibly higher than that of the persistent emission at  $2.6\sigma$  level. Based on these measurements, average wide-band properties of these relatively weak bursts are compared with those of the persistent emission.

**Key words:** stars: pulsars individual(SGR 0501+4516)

## 1. Introduction

Magnetars, comprising Soft Gamma Repeaters (SGRs) and Anomalous X-ray Pulsars (AXPs), have been brought to great attention because they are likely to have super strong surface magnetic fields reaching  $B \sim 10^{15}$  G (Duncan & Thompson 1992; Paczyński 1992; Thompson & Duncan 1995; Thompson & Duncan 1996). This exceeds the critical field strength  $B_c \equiv m_e^2 c^3 / e \hbar \approx 4.4 \times 10^{13}$  G, where  $m_e$ ,  $c$ ,  $e$ , and  $\hbar$  are the electron mass, the light velocity, the electron charge and the reduced Planck constant, respectively. To understand radiation processes in such an environment, it is necessary to fully take into account non-perturbative effects in quantum electrodynamics.

Outstanding properties of magnetars include burst activity, observed from all SGRs and some AXPs. A typical “short burst” has a duration of  $\sim 100$  ms, and a 2–100 keV energy release by  $10^{40-42}$  erg (e.g., Nakagawa et al. 2007). Among a variety of burst activities, the most energetic ones are the giant flares, which were so far detected from SGR 0526–66 (e.g., Mazets, Golenetskii & Gur’yan 1979), SGR 1900+14 (e.g., Hurley et al. 1999b), and SGR 1806–20 (e.g., Palmer et al. 2005).

X-ray spectra of short bursts provide useful diagnostics of their emission mechanism. Wide-band spectra of short bursts from SGR 1806–20 and SGR 1900+14, detected by High Energy Transient Explorer 2 (HETE-2; Ricker et al. 2003), are generally described by a photoelectrically

absorbed two-blackbody (2BB) model (Nakagawa et al. 2007), even though this could be a phenomenological description. Spectra of bursts (Feroci et al. 2004) and intermediate flares (Olive et al. 2004; Israel et al. 2008) from SGR 1900+14 also favor the 2BB modeling. In addition, bursts from the new magnetar SGR 0501+4516, detected by Suzaku (Mitsuda et al. 2007) and Swift (Gehrels et al. 2004), also exhibited 2BB-type spectra (Enoto et al. 2009, hereafter Paper I; Kumar, Ibrahim, Safi-Harb 2010). In terms of this modeling, these short bursts all exhibit an interesting scaling as  $kT_{\text{HT}} \sim 3kT_{\text{LT}}$  (Nakagawa et al. 2007), where  $kT_{\text{HT}}$  and  $kT_{\text{LT}}$  are the higher and lower temperatures of the 2BB model, respectively.

It has long been known that SGRs and AXPs show not only burst activities but also persistent emission in energies below  $\sim 10$  keV, of which the spectra are generally reproduced by two phenomenological models; 2BB (e.g., Tiengo et al. 2008; Nakagawa et al. 2009) or a photoelectrically absorbed blackbody plus power law model (BB+PL; e.g., Marsden & White 2001; Mereghetti, Esposito & Tiengo 2007). Moreover, recent studies of SGR 0501+4516 and other objects propose a “blackbody plus Comptonized blackbody” model (Enoto et al. 2010a, hereafter Paper II) and a resonant cyclotron scattering model (Rea et al. 2008) as alternative possibilities. Although the spectral modeling is thus ambiguous, the persistent X-ray emission interestingly shows the same  $kT_{\text{HT}} \sim 3kT_{\text{LT}}$  relation as those of the bursts (Nakagawa et al. 2009) if we employ the 2BB representation. This sug-

gests a common radiation mechanism between the bursts and persistent emission, further leading to a possibility that the persistent X-ray emission may consist of numerous micro bursts (Nakagawa et al. 2009).

Recent studies using INTEGRAL (e.g., Kuiper, Hermsen, Mendez 2004; Molkov et al. 2005; Rea et al. 2009) and Suzaku (Esposito et al. 2007; Nakagawa et al. 2009; Paper II; Enoto et al. 2010b; Enoto et al. 2010c) revealed an extremely hard X-ray component above  $\sim 10$  keV in persistent emission spectra of a significant fraction of SGRs (including SGR 0501+4516: Paper II) and AXPs. The hard X-ray component, which is thought to be distinct from the blackbody-like soft component, can be reproduced by a power law (PL) model with an extremely hard photon index of  $\Gamma \sim 1$ . As reported in Paper II for SGR 0501+4516 and in Enoto et al. (2010c) for some other sources, the 2–100 keV luminosity of the hard X-ray component is often comparable to that of the soft blackbody component. Considering these properties, as well as a clear dependence of the hardness ratio between the hard and soft luminosities on the characteristic age as revealed with Suzaku (Enoto et al. 2010c), the hard X-ray component is expected to provide an important clue to the nature of magnetars. Theoretically, the hard X-ray production mechanism is extensively discussed (Heyl & Hernquist 2005; Thompson & Beloborodov 2005; Baring & Harding 2007), but it is not yet conclusive.

If there is a common radiation mechanism between the bursts and persistent emissions, the hard X-ray component may also be seen in burst spectra. However, short bursts of magnetars so far studied, with fluence  $> 10^{-8}$  erg cm $^{-2}$ , generally have  $kT_{\text{HT}} = 7\text{--}15$  keV (e.g., Feroci et al. 2004; Nakagawa et al. 2007; Israel et al. 2008; Kumar, Ibrahim, Safi-Harb 2010). As a result, their 2BB spectra, extending well up to  $\gg 10$  keV, would mask any hard X-ray component. This raises a possibility that bursts with considerably lower fluence, which have remained not much studied, may have lower values of  $kT_{\text{HT}}$ , e.g., close to those found in the persistent emission (e.g.,  $kT_{\text{HT}} = 0.4\text{--}3.9$  keV; Tiengo et al. 2008; Nakagawa et al. 2009; Paper II), and would allow more sensitive searches for the hard-tail component. Considering this, we focus on wide-band spectroscopy of low-fluence bursts. Observations with Suzaku are suitable for this purpose, because of its high sensitive over a broad energy band, realized by the X-ray Imaging Spectrometer (XIS; 0.2–12 keV; Koyama et al. 2007) and the Hard X-ray Detector (HXD; 10–600 keV; Takahashi et al. 2007). We have hence revisited the Suzaku data of SGR 0501+4516, acquired during its 2008 August activity. As a third publication (after Paper I and Paper II) from this observation, the present paper reports on our successful detection of a hard component, in an HXD spectrum which sums over 31 short bursts from this new magnetar.

## 2. Observations and Data Reductions

The new soft gamma repeater SGR 0501+4516 was discovered on 2008 August 22 by the burst alert telescope on-board Swift, when it displayed SGR-like burst activ-

ity (Barthelmy et al. 2008). Soon after the discovery, a spin period of  $P = 5.769 \pm 0.004$  was reported based on an observation by the Rossi X-ray Timing Explorer (Göğüş et al. 2008). As described in Paper I and Paper II, we triggered a Suzaku Target-of-Opportunity (ToO) observation, which started at 00:05 on 2008 August 26 and ended at 08:25 on 2008 August 27 (UT). The XIS was operated with a 1/4 window option which yields a 2 s time resolution, while the HXD was operated in the standard mode. The acquired data were already utilized in Paper I and Paper II; the former described a strong short burst and persistent soft X-ray emission, while the latter focused on the detection of a hard component in the persistent emission. The present paper, utilizing the same ToO data, deals with broad-band spectra of 31 smaller short bursts. The distance to SGR 0501+4516, though estimated to be 1.5 kpc based on its directional proximity to the young supernova remnant HB9 (Leathy & Aschenbach 1995; Gaensler et al. 2008), is actually very uncertain. In this paper, the distance is hence assumed to be 4 kpc, which is similar to the value of  $\sim 5$  kpc employed by Rea et al. (2009).

The reduction of the XIS and HXD event data (v2.2) were made using HEASoft 6.6.1 software. The latest calibration database (CALDB: 20090402) was applied to unfiltered XIS event data using *xispi* (v2008-04-10). Then, using *xselect* (v2.4a), we extracted a new set of filtered XIS events with the standard criteria<sup>1</sup> and a grade selection “GRADE = (0,2-4,6)”. After that, hot and flickering pixels were removed using *cleansis* (v1.7). Telemetry-saturated time intervals, estimated by *xisgtigen* (v2007-05-14), were removed from the XIS data using *xselect*. We created light curves and spectra from the cleaned XIS event data using *xselect*. Response matrix files were generated by *xisrmfgen* (v2007-05-14), and ancillary response function files by *xissimarfgen* (v2008-04-05). The obtained net exposure is  $\sim 60$  ks.

Using *hxdpi* and *hxdgrade* (v2008-03-03), we applied the latest calibration database (CALDB: 20090902) to the unfiltered HXD event data. Cleaned PIN and GSO events were extracted from these newly calibrated data with the standard criteria<sup>2</sup> using *xselect*. Again, we created light curves and spectra using *xselect*. Dead time corrections were applied to the spectra using *hxdtdcor*. Response matrix files of version 2008-01-29 were used. This yielded a net exposure of  $\sim 59$  ks for the HXD data.

## 3. Data Analysis

### 3.1. Burst Detections

As shown in figure 1 of Paper I, a number of visually obvious bursts are found in a 0.2–12 keV XIS light curve with 2-s resolution, obtained by summing the data from the two FI sensors (XIS0 and XIS3) and the one BI sensor (XIS1). At least three of them, including the strongest

<sup>1</sup> The XIS standard criteria were derived from <http://suzaku.gsfc.nasa.gov/docs/suzaku/analysis/abc>.

<sup>2</sup> The HXD standard criteria were taken from [http://www.astro.isas.ac.jp/suzaku/analysis/7step\\_HXD\\_20080501.txt](http://www.astro.isas.ac.jp/suzaku/analysis/7step_HXD_20080501.txt).

one analyzed in Paper I, were also noticed in the 10–20 keV HXD-PIN light curve with a 500 ms time resolution. Following our preliminary attempt in Paper I, we conducted a quantitative burst search using the 0.2–12 keV light curve of the XIS. After visually eliminating 8 obvious bursts which have  $> 50 \text{ cts (2 s)}^{-1}$ , the light curve was converted to a count-rate (per 2 s) histogram as shown in figure 1; this includes the background, the persistent signal emission, and short bursts. The histogram has an average of  $\lambda = 12.12 \pm 0.06$  and a standard deviation of  $\sigma = 3.48 \pm 0.01$ , both in units of  $\text{cts (2 s)}^{-1}$ , where the quoted errors refer to 90% confidence levels, and can be approximated by a Poissonian distribution.

We searched the XIS count-rate histogram for those 2-s bins where the count rate exceeds  $\lambda + 5\sigma \sim 30 \text{ cts (2 s)}^{-1}$ . This selection has yielded 35 time bins with significant excess counts. Regarding a set of consecutive such bins as representing a single burst, we thus detected 32 short bursts altogether. Among them, the strongest one was already analyzed in Paper I. Below, we therefore analyze the remaining 31 bursts, which are summarized in table 1. They are hereafter identified sequentially as #01, #02, ..., and #31. These 31 short bursts are considered to be free from event pile-up effects in the XIS, because their count rates were less than  $107 \text{ cts (2 s)}^{-1} \text{ XIS}^{-1}$  above which the effect becomes significant<sup>3</sup>. Light curves of typical short bursts (#03, #13, #14, #22 and #23) are presented in figure 2. Among them, two (#03 and #14) are accompanied by significant emissions in the HXD-PIN and/or HXD-GSO energy bands.

### 3.2. Derivation of On-burst and Background Spectra

Since the present paper puts its focus on burst spectra, we must subtract the persistent emission of SGR 0501+4516, as well as the non X-ray background and the cosmic X-ray background. For each burst, we therefore accumulate the XIS and HXD data over a time region (see below) containing the burst, and subtract the corresponding background spectra which are acquired before and after the burst period. The on-burst and background data of the XIS were both extracted from box regions with sizes of (DETX, DETY) = (260", 360") for XIS1, and (360", 260") for XIS0 and XIS3, where DETX and DETY are detector coordinates.

Each on-burst spectrum was made using a 2-s or 6-s time interval, depending on the burst duration in the XIS. The corresponding background spectra were extracted from two 10-s time intervals, one before and the other after the burst, both separated by 2 s from the on-burst time region. The result does not change if we instead employ 15 s for the background time intervals. Therefore, the pulsed persistent emission with a period of  $\sim 5.76 \text{ s}$  (Paper I) does not affect the background spectrum. If the background time intervals contained other bursts, they were eliminated from the background spectra.

Figure 3 shows 6-band synthetic light curves summed

over the 31 short bursts, obtained by stacking their individual light curves in reference to the 0.2–12 keV XIS data. Thus, the burst emission is clearly seen in the HXD-PIN data up to 40 keV, and possibly in the 50–100 keV HXD-GSO band. Average on-burst and background count-rates of the XIS are  $\sim 53 \text{ cts (2 s)}^{-1}$  and  $\sim 14 \text{ cts (2 s)}^{-1}$ , respectively. Since the XIS have a time resolution of 2 s, the burst profiles in the HXD energy bands in figure 3 must be considerably smeared out.

### 3.3. Spectral Analyses

Figure 4 shows on-burst (*green*), background (*red*), and background subtracted (*black*) spectra of the XIS and the HXD, summed over the 31 bursts. In agreement with figure 3, the burst emission is significantly detected with HXD-PIN up to  $\sim 40 \text{ keV}$ . Also, the burst signal may be detected marginally in the 50–100 keV GSO data.

Before quantifying the burst spectrum, let us compare it with that of the persistent emission of SGR 0501+4516. To do this in a model-independent manner, we directly divided the summed burst spectrum to the background-subtracted persistent-component spectrum derived in Paper II. The ratio in the XIS range was estimated using the two FI sensors. The results, presented in figure 5, indicate that the burst spectrum is clearly harder than the persistent emission spectrum. In addition, the ratio in the HXD range is approximately flat, implying that in this energy range the burst and persistent emission have approximately the same spectral shape.

Using XSPEC 12.5.0 (Arnaud 1996), we fitted the summed burst spectrum with a photoelectrically absorbed 2BB model, which has been most successful on the short bursts from SGR 1806–20 and SGR 1900+14 (section 1). The photoelectric absorption was fixed to  $8.9 \times 10^{21} \text{ cm}^{-2}$ , as estimated from the persistent X-ray emission observed by the XIS (Paper I). According to a cross-calibration between the XIS and the HXD described in Kokubun et al. (2007), the HXD normalization is typically 13% higher than that of the XIS for Crab data acquired at the XIS nominal position. Therefore the relative normalization of the HXD above the XIS was fixed to 1.13. As shown in figure 6 (b), this 2BB fits leaves significant positive residuals in energies above  $\sim 20 \text{ keV}$ , which makes the fit unacceptable with  $\chi^2/\text{d.o.f.} = 74/50$ . Although the 2BB fit could be improved to  $\chi^2/\text{d.o.f.} = 67/49$  by allowing to vary the HXD vs. XIS relative normalization, the obtained normalization ratio,  $0.2_{-0.1}^{+0.2}$ , is far outside the value of  $1.13 \pm 0.03$  obtained from Crab observations (Kokubun et al. 2007), making the fit unrealistic. Conversely, the 2BB fit did not improve significantly if the HXD normalization is kept within this uncertainty range.

Given figure 5, as well as the failure of the 2BB model, we fitted the burst spectrum with a 2BB plus power law model (2BB+PL). The fit was then improved to  $\chi^2/\text{d.o.f.} = 56/48$ . The PL component is considered to be significant, because an F-test indicates a probability of  $\sim 0.1\%$  for the fit improvement (by adding PL) to arise by chance. The best-fit spectral parameters are summarized in table 2, and the  $\nu F_\nu$  form of the 2BB+PL fit is given in

<sup>3</sup> The document is available at [ftp://legacy.gsfc.nasa.gov/suzaku/nra\\_info/suzaku\\_td.pdf](ftp://legacy.gsfc.nasa.gov/suzaku/nra_info/suzaku_td.pdf).

figure 6 (d). As already expected from figure 5, the power-law component indeed exhibits a photon index of  $\Gamma \sim 1$ , which is comparable to that of the hard X-ray component of the persistent emission (e.g., Paper II). Consequently, we conclude that the summed short burst spectrum has a hard-tail component, which has never been detected in the burst spectra of any other magnetar.

Using the best-fit 2BB+PL spectral parameters, a bolometric fluence of the 2BB component and a 2–40 keV fluence of the PL component are calculated as shown in table 2. Those fluences refer to average values of the 31 short bursts, and are lower by two orders of magnitude than a typical 2–100 keV fluence of  $\sim 2 \times 10^{-7}$  erg cm $^{-2}$  for short bursts from SGR 1806–20 and SGR 1900+14 (e.g., Feroci et al. 2004; Nakagawa et al. 2007) studied so far. Thus, the high sensitivity of Suzaku allowed us to study, for the first time, the wide-band properties of these low-fluence bursts. Assuming the effective duration of the 31 short bursts from SGR 0501+4516 to be 0.1 s, which is a typical value for this type of events (e.g., Feroci et al. 2004; Nakagawa et al. 2007), we calculated the flux (luminosity) and the blackbody radii, all averaged over the 31 short bursts, and show the results in table 2. The effective emission radii of the two BB components,  $\sim 14$  km and  $\sim 1.9$  km (assuming a distance of 4 kpc), are comparable to typical values found in short bursts from SGR 1806–20 and SGR 1900+14 (Nakagawa et al. 2007), and from SGR 0501+4516 (Kumar, Ibrahim, Safi-Harb 2010), although the distance uncertainty remains.

#### 4. Discussion and Conclusion

Using the Suzaku ToO observation of SGR 0501+4516 conducted in 2008 August, we studied relatively dim 31 short bursts from this new magnetar. Their average fluence,  $1.0_{-0.5}^{+0.3} \times 10^{-9}$  erg cm $^{-2}$  in 2–40 keV, is 1–2 orders of magnitude lower than those of typical short burst studied so far (e.g., Nakagawa et al. 2007; Israel et al. 2008; Kumar, Ibrahim, Safi-Harb 2010). Following the detection of a hard component from the persistent emission of SGR 0501+4516 (Paper II; Rea et al. 2009), the data have allowed a clear detection of a similar hard-tail component in the spectrum summed over the 31 short bursts. These results for the first time reveal spectral properties of such dim bursts, and provide a new clue to the formation mechanisms of persistent and burst emissions from magnetars.

As already reported in Paper I, the spectrum of the strongest burst (actually its precursor) from SGR 0501+4516 was well reproduced by a 2BB model, without indication of an additional hard X-ray component. However, this could be due to the effect mentioned in section 1, namely, obscuration by the high 2BB temperatures ( $kT_{\text{HT}} \sim 14$  keV); the data of this strong precursor are worth searching for a hard tail component. Therefore, we re-analyzed the same pile-up and dead-time corrected spectrum of the precursor as studied in Paper I, using the 2BB+PL model. The photon index was fixed to  $\Gamma = 1$  to emulate the results obtained in subsection 3.3, and

the photoelectric absorption was again fixed to  $8.9 \times 10^{21}$  cm $^{-2}$  after Paper I. The fit resulted in  $\chi^2/\text{d.o.f.} = 40.1/37 = 1.09$ , which is no better than the value of  $41.2/38 = 1.08$  using the 2BB model. Therefore, the data do not require any excess hard-tail component with  $\Gamma = 1.0$ . The best-fit spectral parameters are summarized in table 2, which are consistent with the results in Paper I after renormalizing to the distance of 4 kpc and the duration of 0.2 s. There, the 2–100 keV flux of the PL component is given as a 90% upper limit.

Given the gross spectral similarity between the short bursts and the persistent emission of SGR 0501+4516 (subsection 3.3), let us perform more quantitative comparison among their soft components, referring to figure 7 which summarizes three sets of 2BB parameters of SGR 0501+4516; the persistent emission, the 31 short bursts, and the precursor of the strongest burst. There, we find three properties that are common to all the three spectra. One is that the cooler and hotter blackbodies have comparable luminosities, and another is that  $kT_{\text{HT}}$  is  $\sim 3$  times higher than  $kT_{\text{LT}}$ . These 2BB properties are considered rather intrinsic to magnetars, because they also apply to more energetic (typically by an order of magnitude in bolometric fluence) bursts from SGR 1806–20 and SGR 1900+14 observed with HETE-2 (figure 5 of Nakagawa et al. 2009), SGR 1900+14 observed with Swift (Israel et al. 2008), and SGR 0501+4516 observed with Swift (Kumar, Ibrahim, Safi-Harb 2010), as well as to persistent emission from some other magnetars (Nakagawa et al. 2009 and references therein). The remaining property found in figure 7 is that the two temperatures increase with the luminosity. In fact, the temperature of the 31 short bursts are by a factor of 4–9 lower than those of the typical bursts (e.g., Feroci et al. 2004; Nakagawa et al. 2007; Israel et al. 2008; Kumar, Ibrahim, Safi-Harb 2010). This justifies a posteriori our conjecture made in section 1, i.e., a positive temperature-luminosity correlation of the 2BB component. Incidentally, the ratio increase in figure 5, from a few keV to  $\sim 10$  keV, is at least partially due to the higher 2BB temperatures of the dim bursts than those of the persistent emission.

In contrast to the present results, some published results (e.g., Kumar, Ibrahim, Safi-Harb 2010) suggest a weak negative correlation between the 2BB temperatures and the burst fluence. However, these results are usually limited to rather strong bursts with fluence  $> 10^{-8}$  erg cm $^{-2}$ . Then, the temperature vs. fluence might change at about this fluence. Alternatively, weaker bursts in these studies may have actually contained hard-tail components, and hence their spectra appeared rather hard.

In addition to these similarities in the soft component, the presence of a distinct PL-shaped hard component, found in the present work, provides a novel resemblance between the 31 short bursts and the persistent emission. Moreover, the photon index of the former,  $\Gamma = 1.0_{-0.3}^{+0.4}$ , is consistent with the latter,  $\Gamma = 1.33_{-0.16}^{+0.23}$  (Paper II). However, as already visualized by figure 5, the two phenomena can differ in their ratios between the 2–40 keV hard-component luminosity  $L_{\text{PL}}$  and the bolometric

soft-component luminosity  $L_{2BB}$ , even excluding the effect caused by different BB temperatures. We observed  $L_{PL}/L_{2BB} = 2.7 \pm 0.9$  from the 31 short bursts, which is possibly higher than that of  $0.36 \pm 0.02$  for the persistent emission at  $2.6\sigma$  level. Here, quoted errors are 68% confidence levels for the ratios, and 90% confidence levels for the photon indices.

In order to visualize the wide-band spectral hardness, we compare in figure 8 the relations between  $L_{PL}$  and  $L_{2BB}$ . There,  $L_{PL}$  was calculated again in the 2–40 keV range. Even though the  $L_{PL}/L_{2BB}$  ratio could vary to some extent, a fact of basic importance is that  $L_{PL}$  and  $L_{2BB}$  increases, by about 2 orders of magnitude in an approximate proportion, from the persistent emission to the dim short bursts. This, together with the spectral similarities discussed above, suggests that common emission mechanisms operate between these short bursts and the persistent emission. This in turn gives a support to our idea that persistent X-ray emission of magnetars may in general consist of numerous micro-bursts (Nakagawa et al. 2009). In contrast, the upper limit on the  $L_{PL}/L_{2BB}$  ratio obtained for the strongest burst is considerably lower than is extrapolated from the other two less luminous data points, suggesting some changes in the emission mechanism from weaker to stronger short bursts.

This work was partially supported by Japan Society for the Promotion of Science (JSPS) KAKENHI Grant-in-Aid for Young Scientists (B) 21740207 and Grant-in-Aid for Scientific Research (A) 22244034.

## References

- Arnaud, K. A. 1996, in *Astronomical Data Analysis Software and Systems V*, eds. G. Jacoby and J. Barnes, ASP Conference Series, 101, 17
- Baring, M. G., & Harding, A. K. 2007, *Ap&SS*, 308, 109
- Barthelmy, S. D. et al. 2008, *GRB Coord. Netw. Circ.*, 8113
- Duncan, R., & Thompson, C. 1992, *ApJ*, 392, L9
- Enoto, T. 2010, Ph.D. Thesis, University of Tokyo
- Enoto, T. et al. 2009, *ApJ*, 693, L122
- Enoto, T. et al. 2010a, *ApJ*, 715, 665
- Enoto, T. et al. 2010b, *PASJ*, 62, 475
- Enoto, T. et al. 2010c, *ApJ*, 722, L162
- Esposito, P. et al. 2007, *A&A*, 476, 321
- Feroci, M., Calliandro, G. A., Massaro, E., Mereghetti, S., & Woods, P. M. 2004, *ApJ*, 612, 408
- Gaensler, B. M., et al. 2008, *GRB Coord. Netw. Circ.*, 8149
- Göğüş, E., Woods, P., & Kouveliotou, C. 2008, *GRB Coord. Netw. Circ.*, 8118
- Gehrels, N., et al. 2004, *ApJ*, 611, 1005
- Heyl, J. S., & Hernquist, L. 2005, *MNRAS*, 362, 777
- Hurley, K., et al. 1999, *Nature*, 397, 41
- Israel, G. L., et al. 2008, *ApJ*, 685, 1114
- Kokubun, M., et al. 2007, *PASJ*, 59, 53
- Koyama, K., et al. 2007, *PASJ*, 59, S23
- Kuiper, L., Hermsen, W., & Mendez, M. 2004, *ApJ*, 613, 1173
- Kumar, H. S., Ibrahim, A. I., & Safi-Harb, S. 2010, *ApJ*, 716, 97
- Leathy, D. A., & Aschenbach, B. 1995, *A&A*, 293, 853
- Marsden, D., & White, N. E. 2001, *ApJ*, 551, L155

- Mazets, E. P., Golenetskii, S. V., & Gur'yan, Yu. A. 1979, *Soviet Astron. Lett.*, 5, 343
- Mereghetti, S., Esposito, P., & Tiengo, A. 2007, *Ap&SS*, 308, 13
- Mitsuda, K., et al. 2007, *PASJ*, 59, S1
- Molkov, S., Hurley, K., Sunyaev, R., Shtykovsky, P., Revnivtsev, M., & Kouveliotou, C. 2005, *A&A*, 433, L13
- Nakagawa, Y. E., et al. 2007, *PASJ*, 59, 653
- Nakagawa, Y. E., et al. 2008, *GRB Coord. Netw. Circ.*, 8265
- Nakagawa, Y. E., et al. 2009, *PASJ*, 61, S387
- Olive, J. -F. et al. 2004, *ApJ*, 616, 1148
- Paczyński, B. 1992, *Acta Astron.*, 42, 145
- Palmer, D. M., et al. 2005, *Nature*, 434, 1107
- Rea, N., Zane, S., Turolla, R., Lyutikov, M., Götz, D. 2008, *ApJ*, 686, 1245
- Rea, N., et al. 2009, *MNRAS*, 396, 2419
- Ricker, G., et al. 2003, in *Gamma-Ray Bursts and Afterglow Astronomy*, ed. G. R. Ricker & R. Vanderspek (Melville: AIP), 662, 3
- Takahashi, T., et al. 2007, *PASJ*, 59, S35
- Tanaka, Y. T., Terasawa, T., Yoshida, M., Horie, T., Hayakawa, M. 2008, *J. Geophys. Res.*, 113, A07307
- Thompson, C., & Beloborodov, A. M. 2005, *ApJ*, 634, 565
- Thompson, C., & Duncan, R. 1995, *MNRAS*, 275, 255
- Thompson, C., & Duncan, R. 1996, *ApJ*, 473, 322
- Tiengo, A., Esposito, P., & Mereghetti, S. 2008, *ApJ*, 680, 133

**Table 1.** A summary of 31 short bursts from SGR 0501+4516 detected by Suzaku.

Burst	Date (UT)*	XIS Counts <sup>†</sup>
#01	2008-08-26 01:05:44	35
#02	2008-08-26 01:07:02	30
#03	2008-08-26 01:23:20	309
#04	2008-08-26 01:24:08	42
#05	2008-08-26 01:30:22	38
#06	2008-08-26 02:43:44	34
#07	2008-08-26 02:46:02	61
#08	2008-08-26 02:46:48	30
#09	2008-08-26 02:50:24	32
#10	2008-08-26 02:50:38	36
#11	2008-08-26 03:16:32	33
#12	2008-08-26 03:16:54	37
#13	2008-08-26 03:21:00	240
#14	2008-08-26 03:21:08	99
#15	2008-08-26 03:21:26	30
#16	2008-08-26 04:38:10	35
#17	2008-08-26 08:00:58	30
#18	2008-08-26 09:25:06	31
#19	2008-08-26 10:47:32	42
#20	2008-08-26 12:45:34	66
#21	2008-08-26 12:45:42	50
#22	2008-08-26 14:22:50	66
#23	2008-08-26 14:22:58	33
#24	2008-08-26 15:27:48	30
#25	2008-08-26 15:27:56	33
#26	2008-08-26 15:44:14	32
#27	2008-08-26 22:26:44	30
#28	2008-08-27 06:07:02	33
#29	2008-08-27 07:55:40	38
#30	2008-08-27 07:55:48	31
#31	2008-08-27 07:55:56	34

\* A central time of the first 2-s bin of each short burst.

† Counts in a 0.2–12 keV band. The burst 13 has a 6-s duration, while the others has a 2-s duration.

**Table 2.** Fit results of the Suzaku spectra summed over the 31 short bursts and the strongest burst precursor.\*

Model	$kT_{\text{LT}}^{\dagger}$ (keV)	$R_{\text{LT}}^{\ddagger}$ (km)	$kT_{\text{HT}}^{\dagger}$ (keV)	$R_{\text{HT}}^{\ddagger}$ (km)	$\Gamma^{\S}$	$S_{2\text{BB}}^{\parallel}$	$S_{\text{PL}}^{\parallel}$	$F_{2\text{BB}}^{\#}$	$F_{\text{PL}}^{\#}$	$\chi^2/\text{d.o.f.}$
The 31 Short Bursts										
2BB	$0.61 \pm 0.14$	$(12_{-3}^{+6})t_{0.1}^{-0.5}$	$2.6_{-0.7}^{+0.9}$	$(1.2_{-0.4}^{+0.9})t_{0.1}^{-0.5}$	...	$0.60_{-0.10}^{+0.18}$	...	$(0.60_{-0.10}^{+0.18})t_{0.1}^{-1}$	...	74/50
2BB+PL	$0.49_{-0.08}^{+0.10}$	$(14_{-2}^{+5})t_{0.1}^{-0.5}$	$1.7 \pm 0.3$	$(1.9_{-0.6}^{+0.7})t_{0.1}^{-0.5}$	$1.0_{-0.3}^{+0.2}$	$0.26 \pm 0.12$	$0.7 \pm 0.3$	$(0.26 \pm 0.12)t_{0.1}^{-1}$	$(0.7 \pm 0.3)t_{0.1}^{-1}$	56/48
The Strongest Burst Precursor										
2BB+PL	$3.3 \pm 0.3$	$6.9 \pm 0.7$	$14.3_{-2.0}^{+2.6}$	$0.45_{-0.13}^{+0.16}$	1.0 (fixed)	$190 \pm 30$	$< 20$	$100 \pm 20$	$< 10$	40/36

\* The precursor duration of 0.2 s is assumed. The photoelectric absorption is fixed to  $8.9 \times 10^{21} \text{ cm}^{-2}$ . The distance is assumed to be 4 kpc. The quoted errors are 90% confidence levels.

<sup>†</sup>  $kT_{\text{LT}}$  and  $kT_{\text{HT}}$  denote blackbody temperatures.

<sup>‡</sup>  $R_{\text{LT}}$  and  $R_{\text{HT}}$  denote the emission radii, with  $t_{0.1}$  the burst duration in 0.1 s unit.

<sup>§</sup>  $\Gamma$  denotes the photon index of the PL component.

<sup>||</sup>  $S_{2\text{BB}}$  and  $S_{\text{PL}}$  denote bolometric and 2–40 keV (2–100 keV for the precursor) fluence of the 2BB and PL components, respectively, in units of  $10^{-9} \text{ erg cm}^{-2}$ .

<sup>#</sup>  $F_{2\text{BB}}$  and  $F_{\text{PL}}$  are fluxes corresponding to  $S_{2\text{BB}}$  and  $S_{\text{PL}}$  respectively, in units of  $10^{-8} \text{ erg cm}^{-2} \text{ s}^{-1}$ .

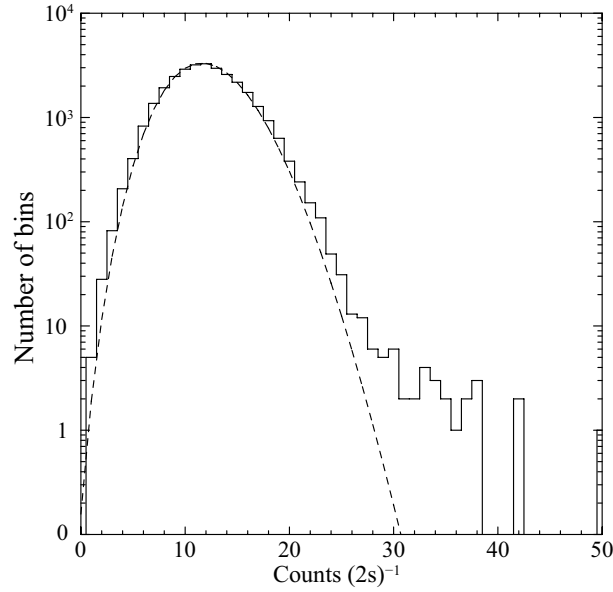


**Fig. 1.** A histogram (solid line) of the 0.2–12 keV XIS counts (per 2 s) of SGR 0501+4516. The dashed line shows the best-fit Poisson distribution with a mean of 12.12 counts  $(2s)^{-1}$ .

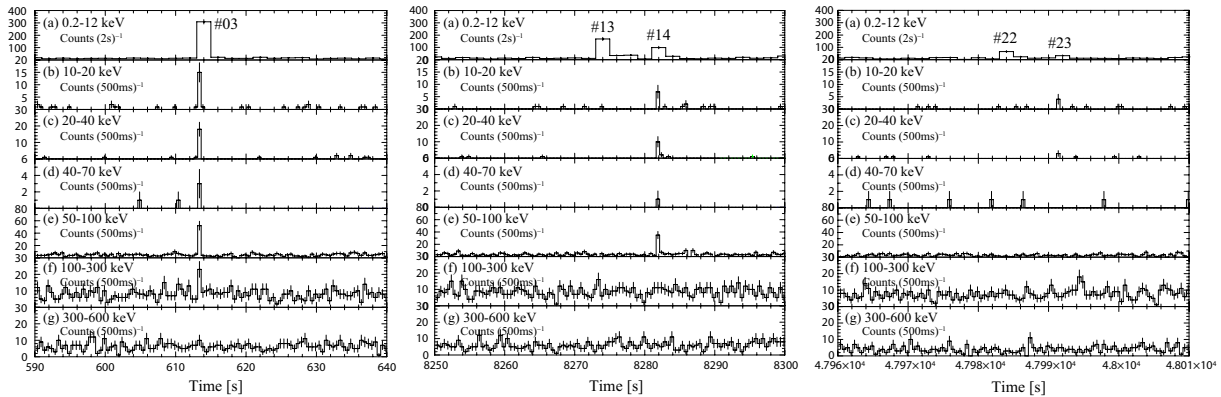


**Fig. 2.** Light curves of five typical short bursts from SGR 0501+4516 recorded with the XIS and the HXD. The time resolution is 2s for the 0.2–12 keV energy band, and 0.5s for the other energy bands. Panels (a) are from the XIS, panels (b)-(d) are from HXD-PIN, while panels (e)-(g) are from HXD-GSO.



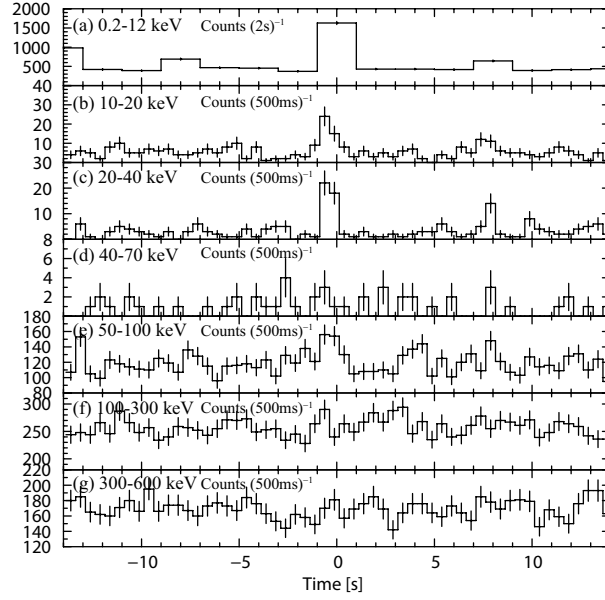


**Fig. 3.** The same as figure 2, but the 31 short bursts are stacked referring to the XIS data.

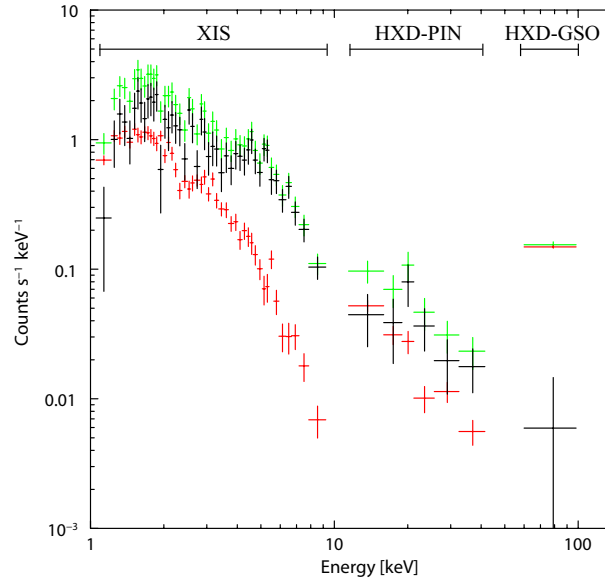


**Fig. 4.** On-burst (green), background (red), and background-subtracted (black) spectra of SGR 0501+4516, summed over the 31 short bursts. The error bars represent statistical  $1\sigma$ .

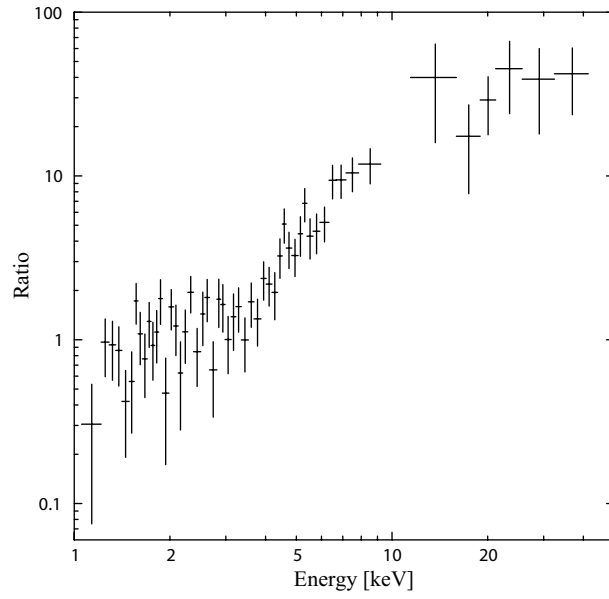


**Fig. 5.** Ratios of the spectrum summed over the 31 short bursts, to that of the persistent emission derived in Paper II. The GSO data are omitted, because the GSO detection of the persistent emission is not significant (Paper II).

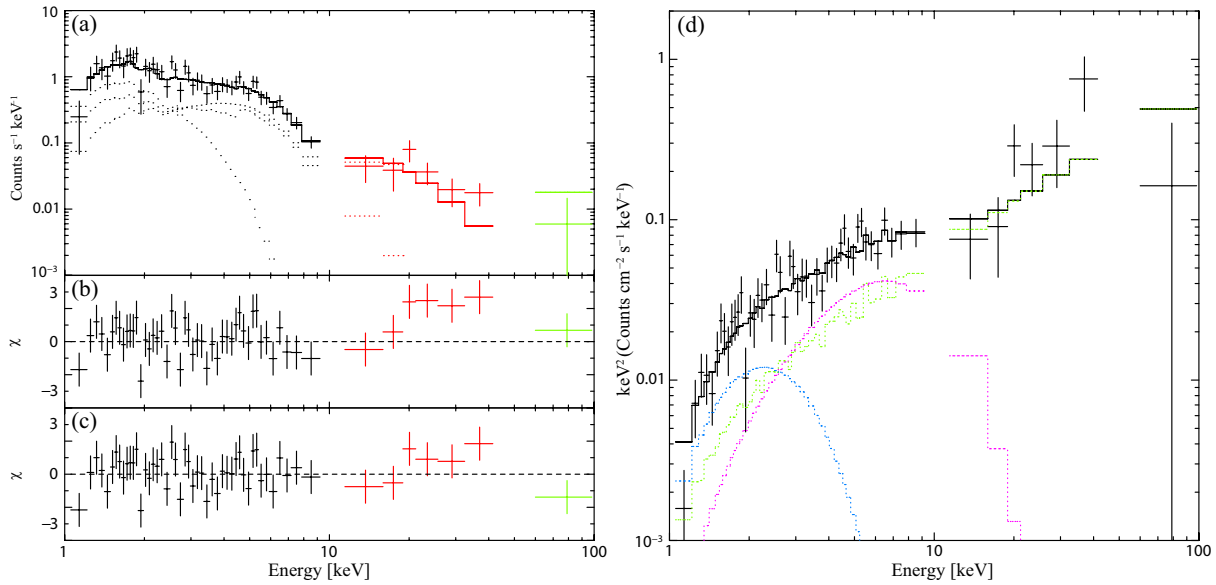


**Fig. 6.** (a) Background-subtracted XIS and HXD spectra of the summed 31 short bursts from SGR 0501+4516, fitted jointly with a 2BB+PL model. Panels (b) and (c) show residuals from the 2BB and 2BB+PL fits, respectively. Panel (d) is the same as panel (a), but in the  $\nu F_\nu$  form.

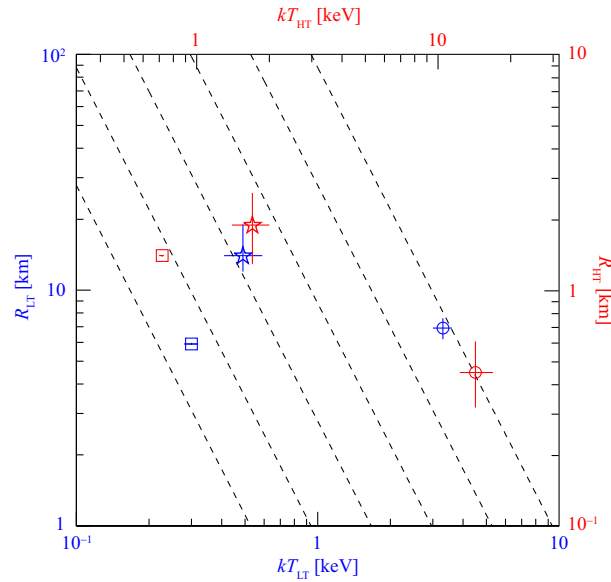


**Fig. 7.** Relations between the temperatures (abscissa) and the emission radii (ordinate) of the 2BB components of SGR 0501+4516. Stars show the 31 short bursts assuming the effective duration of 0.1 s, while circles represent the strongest burst precursor assuming a duration of 0.2 s. Squares indicate the persistent emission (Paper II). Red shows the high temperature component (scales at top and right), while blue the low temperature component (scales at bottom and left). Between the two components, the temperature axes are offset by a factor of  $\sqrt{10}$ , while the radius axes by a factor of 10. Dashed lines indicate contours of bolometric luminosity,  $L$ , which is common to the two blackbody components.

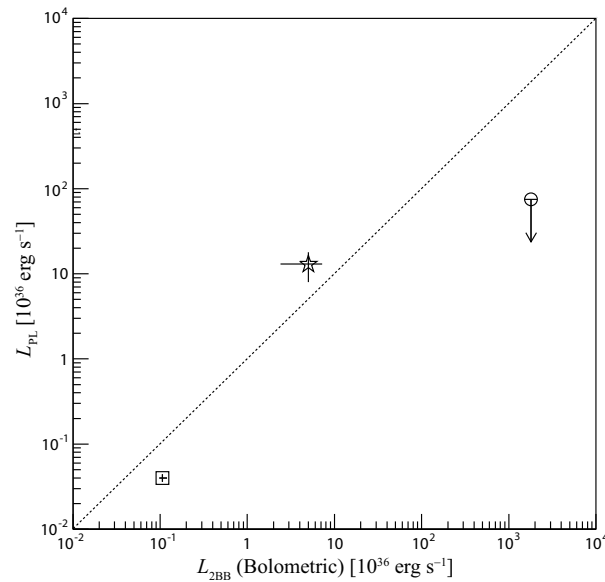


**Fig. 8.** A relation between the bolometric luminosity  $L_{2BB}$  of the 2BB component and the 2–40 keV luminosity  $L_{PL}$  of the PL component, measured with Suzaku from SGR 0501+4516. A star shows the 31 short bursts assuming the effective duration of 0.1 s, an open circle represents the strongest burst precursor, while an open square indicates the persistent emission (Paper II). The dashed line shows  $L_{PL} = L_{2BB}$ . Error bars refer to the 90% confidence limits.